

Superconductivity at 52 K in hydrogen-substituted $\text{LaFeAsO}_{1-x}\text{H}_x$ under high pressure

H. Takahashi^{1,*}, H. Soeda¹, M. Nukii¹, C. Kawashima¹, T. Nakanishi², S. Iimura³, Y. Muraba⁴, S. Matsuishi⁴, and H. Hosono^{3,4}

¹ Department of Physics, College of Humanities and Sciences, Nihon University, Tokyo, Japan

² Department of Physics, School of Science and Technology for Future Life, Tokyo Denki University, Tokyo, Japan

³ Materials and Structures Laboratory, Tokyo Institute of Technology, Yokohama, Japan

⁴ Materials Research Center for Element Strategy, Tokyo Institute of Technology, Yokohama, Japan

* hiroki@chs.nihon-u.ac.jp

The 1111-type iron-based superconductor $\text{LnFeAsO}_{1-x}\text{F}_x$ (Ln stands for lanthanide) is the first material with a T_c above 50 K, other than cuprate superconductors. Electron doping into LaFeAsO by H, rather than F, revealed a double-dome-shaped T_c - x diagram, with a first dome (SC1, $0.05 < x < 0.20$) and a second dome (SC2, $0.2 < x < 0.5$). Here, we report the T_c for the whole hydrogen-doping range in $\text{LaFeAsO}_{1-x}\text{H}_x$ under pressures of up to 19 GPa. T_c rises to 52 K at 6 GPa for the T_c -valley composition between the two T_c domes. This is the first instance of the T_c exceeding 50 K in La-1111-type iron-based superconductors. On the other hand, the T_c of $\text{SmFeAsO}_{1-x}\text{H}_x$ decreased continually, keeping its single-dome structure up to 15 GPa. The present findings strongly suggest that the main reason for realization of the $T_c > 50$ K observed in RE-1111 compounds (RE: Pr, Sm, and Gd) at ambient pressure is the merging of SC1 and SC2.

The discovery of the iron-based superconductor $\text{LaFeAsO}_{1-x}\text{F}_x$ had a significant impact on condensed matter physics as a new platform for studying high- T_c superconductivity¹. Several kinds of materials have been developed, and the highest T_c obtained to date is 58.1 K for Ln-1111-type $\text{LnFeAsO}_{1-x}\text{F}_x$ (Ln stands for lanthanide)². The undoped compound LaFeAsO is a Pauli paramagnetic metal with a tetragonal symmetry at room temperature, and undergoes structural (tetragonal-to-orthorhombic) and magnetic (paramagnetic-to-antiferromagnetic) transitions^{3,4}. Superconductivity appears when both transitions are suppressed with carrier doping. The interplay between superconductivity and magnetism is important, and several models have been proposed

for the appearance of superconducting phase next to the antiferromagnetic phase. For lightly-doped materials, a spin fluctuation resulting from the Fermi surface nesting between hole and electron pockets is a plausible candidate for the pairing mechanism^{5,6}.

Hydrogen-doped Ln -1111 materials were successfully synthesized using the high solubility limit of hydrogen⁷, covering the over-doped region, which has never been studied before because of the low solubility limit of fluorine. A combined study of neutron diffraction measurements with density functional calculations on $LnFeAsO_{1-x}D_x$ demonstrated that these hydrogen atoms are incorporated as H^- ions at the O^{2-} sites. The hydrogen doping causes superconductivity in the same manner as fluorine doping for Sm ⁸, Ce ⁹ and La -1111⁷, as shown in the previous studies. A complete single T_c dome is observed in Ce and Sm -1111⁷, while a double-dome-shaped T_c curve is obtained in $LaFeAsO_{1-x}H_x$, which has hitherto not been observed for Ln -1111. The phase diagrams of $LaFeAsO_{1-x}H_x$ and $SmFeAsO_{1-x}H_x$ at ambient pressure are presented in Fig. 1. The T_c curve of the first dome (SC1) in the lightly-doped region almost coincides with the fluorine-doped La -1111. However, the second dome (SC2) in the heavily-doped region has the maximum T_c of 36 K at $x = 0.36$, which is higher than that of SC1. The SC2 is far from the magnetic phase of $x=0$. This finding suggests that the rigid-band picture does not hold in the highly-doped region^{7,10} because the size and shape of hole pocket on the Fermi surface differs fairly from those of the electron pockets. Thus, orbital fluctuation and/or spin fluctuation resulting from another have been proposed recently as the superconductivity mechanism in the highly-doped region¹⁰. In addition, a new antiferromagnetic phase was recently discovered by NMR¹¹ and neutron diffraction measurements¹² in the over-doped region ($x \sim 0.5$) in $LaFeAsO_{1-x}H_x$, where the T_c of the SC2 vanishes. This magnetic phase is expected to be the key to understanding the appearance of the second T_c dome.

Applying pressure is a very effective means of examining the properties of such layered superconductors. The use of pressure allows the electronic structure to be modified by a physical means, without inducing disorders and/or impurities. A number of important results have been obtained for iron-based superconductors using high-pressure techniques. Applying a pressure of 4 GPa on the first discovered iron-based superconductor $LaFeAsO_{1-x}F_x$ raised the T_c substantially, from 26 K to 43 K¹³. This large pressure effect is recognized as one of the striking features of iron-based superconductors. In addition to the enhancement of T_c , pressure-induced superconductivity has been discovered in, for example, $LaFeAsO$ ¹⁴ and $SrFe_2As_2$ ¹⁵, and a pressure-induced higher- T_c phase has been identified in 11-type iron chalcogenide $FeSe$ ¹⁶. These high-pressure results can provide guiding principles for the development of new superconductors and pave the way to promising new means of investigating iron-based superconductors. High-pressure experiments have already been performed on $LaFeAsO_{1-x}H_x$ at up to 3 GPa, revealing that the double T_c dome (domes SC1 and SC2) merged into a single dome at 3 GPa⁷; however, it remains unclear how this merge occurred. It should also be intriguing to examine what effects are induced by further compression (> 3 GPa).

Here, we study high-pressure effects over the entire hydrogen-doping range in $LaFeAsO_{1-x}H_x$ under pressures of up to 19 GPa. The T_c at the T_c -valley composition between the two T_c domes is greatly increased, from 18 K to 52 K, under a pressure of 6 GPa. This is the first known instance of 50 K being exceeded in a La -1111-type iron-based superconductor. Such a large enhancement in T_c suggests that the two factors giving rise to SC1 and SC2 are effectively merged at the T_c -valley composition, leading

to a higher T_c comparable to those of high- T_c Ln -1111 compounds ($Ln = Nd, Sm, \text{ and } Gd$). These results are compared with the superconducting properties of $SmFeAsO_{1-x}H_x$ under high pressure.

Results

LaFeAsO_{1-x}H_x. Figure 2a shows the temperature dependence of electrical resistance for LaFeAsO_{1-x}H_x with $x = 0.18$ (T_c -valley composition) at each pressure obtained using a diamond anvil cell (DAC). The sudden decrease in resistance in the low temperature range is regarded to be due to the superconducting transition. The onset T_c is given by the intersection of two extrapolated lines, one drawn through the resistance curve for the normal state just above T_c , and the other drawn through the steepest part of the resistance curve for the superconducting state, as shown in Fig. 2a. The pressure dependence of the T_c 's for LaFeAsO_{1-x}H_x with $x = 0.07, 0.18, 0.30, \text{ and } 0.44$ is plotted in Fig. 2b. The T_c 's obtained using a piston-cylinder cell below 2.5 GPa are shown in the same figure. The pressure dependence of T_c for $x = 0.18$ exhibits a dome shape with the maximum T_c of 52 K at 6 GPa. The T_c vs. P curves for the other compositions, with the exception of $x = 0.44$, also show a dome-shaped pressure dependence. The T_c of the heavily-doped LaFeAsO_{1-x}H_x with $x = 0.44$ decreases monotonically with applied pressure. Figure 2d shows the pressure dependence of normalized lattice constants a and c at 60 K and the atomic position of As (z_{As}) estimated by density-functional-theory (DFT) calculations. Although a small discrepancy between the calculated and experimental z_{As} has been reported previously due to the strong electronic correlations¹⁷, it is enough to see the trend of the pressure dependency. It is clear that as the pressure increased, the lattice is compressed and the As-Fe-As angle (α) given by $2\arctan\{a/c \times 1/[2(z_{As} - 0.5)]\}$, decreases monotonically.

SmFeAsO_{1-x}H_x. Figure 3a shows the temperature dependence of electrical resistivity for lightly-doped SmFeAsO_{1-x}H_x with $x = 0.03$ at each pressure obtained using a piston-cylinder cell. The large change in resistivity at around 100 K corresponds to structural and magnetic transitions similar to those reported for LaFeAsO. This transition temperature T_0 is given by the temperature at which $d\rho/dT$ shows its peak value and is suppressed at a rate of -10.0 K/GPa under pressure. On the other hand, a T_c is also observed at around 5 K that increases at a rate of +1.2 K/GPa. The pressure dependence of T_c for SmFeAsO_{1-x}H_x with $x = 0.03, 0.07, 0.10, 0.20, 0.32, 0.34, \text{ and } 0.38$ is shown in Fig 3b. Except for $x = 0.03$, T_c decreases with increasing applied pressure, at rates ranging from -1.2 to -0.6 K/GPa. High-pressure resistance measurements using a DAC are carried out for $x = 0.20$ and 0.38 at up to 15 GPa, in which T_c decreases at the same rate as in the pressure region below 2.5 GPa.

Discussion

In layered materials, the anisotropic contraction usually induces a significant change in the charge distribution, leading to a change in the electronic state. For iron-based superconductors, such a effect may be expected because of the layered structure. Moreover, experimental work has indicated that electronic states are sensitive to the local structure around iron, such as the bond angle and bond length. For 1111-type superconductors, it is widely believed that T_c increases as the FeAs₄ tetrahedron approaches its regular shape having an As-Fe-As bond angle α of 109.47° (so-called

“Lee’s plot”)¹⁸. According to this idea, spin fluctuation is the key ingredient in the glue of the electron pair, since the calculated band structure for the crystal structure having a regular tetrahedron is suitable for the development of spin fluctuation resulting from the Fermi surface nesting between hole and electron pockets.

Figure 4a shows the T_c - x phase diagrams for several pressures up to 13 GPa. Under an applied pressure of 1 GPa, the T_c domes SC1 and SC2 are enhanced, and SC2 shifts to the lightly-doped side, while SC1 shifts in the opposite direction. Increasing the applied pressure to 6 GPa greatly raises the T_c -valley, which causes the double T_c dome to merge into a single T_c dome and to shift to the lightly-doped side as a single T_c dome. The width of this single T_c dome is smaller than the double T_c dome. For hydrogen-doped La-1111 and Sm-1111 (see Fig. 1a), the optimal x indicated by the arrows shifts to the lightly-doped side in the order La to Sm, and the width of the T_c dome is larger for La-1111 than for Sm-1111. However, these features are widely recognized in hydrogen-doped Ln -1111 ($Ln = \text{La, Ce, Sm, and Gd}$), as the ionic radius of Ln decreases in the order $\text{La} > \text{Ce} > \text{Sm} > \text{Gd}$ ⁷. Since the crystal lattice is compressed under pressure, it is reasonable to consider that the double dome T_c in La-1111 would deform and approach the shape of the Sm-1111 single T_c dome under high pressure. Thus, it is plausible that the dramatic rise in T_c to 52 K, observed in the T_c -valley, is attributable to the combined effect of pressure on the two T_c domes. For hydrogen-doped Sm-, Ce-, and Gd-1111, the observed single T_c dome having an optimum T_c above 40 K is presumably a consequence of the effective merge of the two T_c domes. In the case of La-1111, increasing the applied pressure to 13 GPa leads to further shrinkage of the T_c dome. Figure 4b shows the T_c - x phase diagram of $\text{SmFeAsO}_{1-x}\text{H}_x$ for a number of pressures up to 15 GPa. T_c decreases monotonically with pressure, and the single T_c dome shrinks and shifts to the lightly-doped side, as in the case of La-1111 above 6 GPa.

For $\text{LaFeAsO}_{1-x}\text{H}_x$, the power law exponent n of the normal-state electrical resistivity is ~ 2 in the SC1 region, which reflects the Fermi liquid-like properties. On the other hand, in the SC2 region, which has a higher T_c , a non-Fermi liquid-like behavior ($n \approx 1$) was observed. It was indicated that T_c increases as n approaches unity⁷. A T_c above 40 K has also been observed in other hydrogen-doped Ln -1111 for $n \approx 1$. However, for $\text{LaFeAsO}_{1-x}\text{H}_x$ at the T_c -valley composition, n does not change significantly with increasing pressure, despite the dramatic change in T_c from 16 to 52 K under an applied pressure of 6 GPa. Figure 2c shows the pressure dependence of n for the T_c -valley material. The n value decreases very gradually from 2.0 at ambient pressure to unity. The correlation between T_c and n observed at ambient pressure is largely absent in this high-pressure case. This result suggests that under high pressure, the change in the electronic state of $\text{LaFeAsO}_{1-x}\text{H}_x$ is insignificant, while the change in its T_c is large.

Structurally, it is reasonable to consider that under high pressure, the FeAs_4 tetrahedron deforms, stretching in the inter-layer direction. Since the inter-layer bond is not as strong as the covalent Fe-As bond, the former is more susceptible to pressure. Thus, the FeAs_4 tetrahedron stretches in the inter-layer direction when it deforms, as demonstrated in $\text{Ba}(\text{Fe}_{1-x}\text{Co}_x)_2\text{As}_2$ ²⁰. This deformation decreases the As-Fe-As bond angle α . In the case of $\text{LaFeAsO}_{1-x}\text{H}_x$, the decrease of bond angle α with increasing pressure is demonstrated by x-ray diffraction measurements and DFT calculations, as shown in Fig. 2d. These results indicate that hydrogen doping and pressure both cause the tetrahedron to deform and approach a regular tetrahedron. It is revealed that the structure of La1111 approaches to Sm1111 with applying pressure, which is consistent with the pressure

effect on T_c .

The interplay between magnetism and superconductivity in high- T_c cuprates and heavy-fermion materials has been examined since before the discovery of iron-based superconductors. For $\text{LaFeAsO}_{1-x}\text{H}_x$, NMR experiments¹¹ and theoretical calculations¹⁰ indicate that spin and orbital fluctuations develop around the second magnetic ordering phase in the over-doped region. Because theoretical calculations suggest that the spin and orbital fluctuations develop mutually in this system in the lightly- and heavily-doped regions¹⁰, we believe that the large enhancement in T_c to 52 K at the T_c -valley composition is caused by combined effects arising from both SC1 and SC2. Our preliminary measurements show that the second magnetic ordering is suppressed under an applied pressure. We also note that the T_c in the heavily-doped region is suppressed by pressure, while the T_c in the lightly-doped region is enhanced by pressure, when the undoped magnetic phase is suppressed. This suggests that a different relationship exists between the magnetic phase and superconductivity for the two T_c domes.

Recent theoretical calculations have reproduced the double-dome T_c behavior in $\text{LaFeAsO}_{1-x}\text{H}_x$ by considering two kinds of pairing causes for SC1 and SC2^{21,22}. In terms of orbital fluctuation²¹, the approximate s_{++} -wave gap structures due to orbital fluctuations were obtained for both the undoped and over-doped extremes and the double-dome T_c was obtained by switching the dominant quadrupole fluctuation from the SC1 phase (conventional nematic orbital fluctuation) to the SC2 phase (non-nematic orbital fluctuation). On the other hand, the spin fluctuation gives rise to the s_{+-} -wave gap structure. By extending these theoretical considerations, the double-dome T_c curve could be explained through the relationship between next-nearest-neighbor hoppings (t_1) between the d_{xy} orbital of iron sites and second-nearest-neighbor hoppings (t_2)²². For SC1, $t_1 > t_2$ is established, and the spin fluctuation arising from the Fermi surface nesting between electron and hole pockets is thought to play an important role in the superconducting mechanism. By contrast, for SC2, $t_1 < t_2$ and spin fluctuation due to a different cause is thought to be important, leading to the higher T_c maximum. For other hydrogen-doped Ln -1111 materials, a double-dome T_c has not been observed for T_c higher than 40K ($\text{SmFeAs}_{1-x}\text{P}_x\text{O}_{1-y}\text{H}_y$ system has a double dome structure but their optimal $T_c \sim 20$ K²⁶), because $t_1 < t_2$ occurs in the more lightly-doped region. Sm-1111 has a T_c of 56 K at the optimal hydrogen concentration, where the $t_1 < t_2$ condition is thought to be stable. Therefore, we may conclude that the effect of pressure on T_c in Sm-1111 is not as large as it is in La-1111; in La-1111, the two hopping components compete with each other around the T_c -valley composition and are thus sensitive to pressure.

In summary, we measure the pressure dependence of T_c for the whole hydrogen-doping range in $\text{LaFeAsO}_{1-x}\text{H}_x$ under high pressure. The T_c dome of SC2 is enhanced and shifts to the lightly-doped side upon applying pressure. Judging from the phase diagram obtained under high pressure, the SC2 phase becomes dominant in the high-pressure phase. We believe that the enhancement in T_c is caused by a combination of multiple effects. In particular, the two factors giving rise to SC1 and SC2 are effectively merged at the T_c -valley composition, yielding a higher T_c , comparable to those of high- T_c Ln -1111 compounds. The $T_c(x)$ curve is suppressed above 6 GPa, as seen in the phase diagram, similarly to what is observed in the Sm-1111 phase diagram under high pressure. For $\text{SmFeAsO}_{1-x}\text{H}_x$, the two phases of SC1 and SC2 are thought to merge at ambient pressure. High-pressure studies of the magnetic phase on the highly-doped side are important to examine the interplay between superconductivity and magnetism.

Methods

Resistivity measurements under high pressure

Electrical resistivity measurements under high pressure were performed by the standard dc four-probe method. Pressures of up to 2.5 GPa were applied at room temperature using a WC piston and NiCrAl cylinder device. A liquid pressure-transmitting medium (Daphne oil 7474) was used to maintain hydrostatic conditions. A diamond anvil cell (DAC) made of CuBe alloy was used for electrical resistance measurements at pressures up to 30 GPa: in this case, the sample chamber comprising a rhenium gasket was filled with powdered NaCl as the pressure-transmitting medium, and thin (10- μ m-thick) platinum ribbons were inserted into the sample chamber to act as leads for the standard dc four-probe analysis. The dimensions of the samples were 0.1 \times 0.1 \times 0.03 mm. A thin BN layer acted as electric insulation between the leads and the rhenium gasket. Fine ruby powder scattered throughout the sample chamber was used to determine the pressure by the standard ruby fluorescence method. The lack of a measurement of zero resistance in La1111 as shown in Fig. 2a could be due to technical limitations inherent in the experimental apparatus, since fully symmetric hydrostatic compressive stress could not be applied inside the DAC when using a solid pressure-transmitting medium. On the other hand, the resistivity measurement of Sm1111 shows zero resistivity as shown in Fig. 3a, since it was carried out using piston cylinder apparatus, in which liquid pressure-transmitting medium was used to maintain hydrostatic conditions.

Density functional theory calculations

Non-spin-polarized DFT calculations for LaFeAsO_{0.82}H_{0.18} were performed using the projected augmented plane-wave method²³ implemented in the Vienna ab initio simulation program (VASP) code²⁴ and the generalized gradient approximation Perdew–Burke–Ernzerhof functional for solid²⁵. Experimental lattice-constants determined under high pressure were used and plane-wave basis-set cutoff was set to 600 eV. The 10 \times 10 \times 6 meshes were taken for the Brillouin zone integration. For doping-effect, the virtual crystal approximation was used by replacing the oxygen potential with the 0.82:0.18 mixture of oxygen and fluorine potentials. Atomic positions under high pressure were calculated by the structure relaxation with fixed lattice constants.

References

1. Kamihara, Y., Watanabe, T., Hirano, M. & Hosono, H. Iron-based layered superconductor La[O_{1-x}F_x]FeAs ($x=0.05-0.12$) with $T_c=26$ K. *J. Am. Chem. Soc.* **130**, 3296–3297 (2008).
2. Fujioka, M. *et al.* Phase diagram and superconductivity at 58.1 K in α -FeAs-free SmFeAsO_{1-x}F_x. *Supercond. Sci. Technol.* **26** 085023 (2013).
3. de la Cruz, C. *et al.* Magnetic order close to superconductivity in the iron-based layered LaO_{1-x}F_xFeAs systems. *Nature* **453**, 899–902 (2008).
4. Nomura, T. *et al.* Crystallographic phase transition and high- T_c superconductivity in LaFeAsO: F. *Supercond. Sci. Technol.* **21**, 125028 (2008).
5. Mazin, I. I., Singh, D. J., Johannes, M. D. & Du, M. H. Unconventional superconductivity with a sign reversal in the order parameter of LaFeAsO_{1-x}F_x. *Phys. Rev. Lett.* **101**, 05700 (2008).
6. Kuroki, K. *et al.* Unconventional pairing originating from the disconnected fermi

- surfaces of superconducting $\text{LaFeAsO}_{1-x}\text{F}_x$. *Phys. Rev. Lett.* **101**, 087004 (2008).
7. Iimura, S. *et al.* Two-dome structure in electron-doped iron arsenide superconductors. *Nat. Commun.* **3**, 943 (2012).
 8. Hanna, T. *et al.* Hydrogen in layered iron arsenides: Indirect electron doping to induce superconductivity. *Phys. Rev. B* **101**, 024521 (2011).
 9. Matsuishi, S. *et al.* Structural analysis and superconductivity of $\text{CeFeAsO}_{1-x}\text{H}_x$. *Phys. Rev. B* **101**, 014514 (2012).
 10. Yamakawa, Y. *et al.* Phase diagram and superconducting states in $\text{LaFeAsO}_{1-x}\text{H}_x$ based on the multiorbital extended Hubbard model. *Phys. Rev. B* **88**, 041106 (2013).
 11. Fujiwara, N. *et al.* Detection of antiferromagnetic ordering in heavily doped $\text{LaFeAsO}_{1-x}\text{H}_x$ pnictide superconductors using nuclear-magnetic-resonance techniques. *Phys. Rev. Lett.* **111**, 097002 (2013).
 12. Hiraishi, M. *et al.* Bipartite magnetic parent phases in the iron oxy pnictide superconductor. *Nat. Phys.* **10**, 300–303 (2014).
 13. Takahashi, H. *et al.* Superconductivity at 43 K in an iron-based layered compound $\text{LaO}_{1-x}\text{F}_x\text{FeAs}$. *Nature* **453**, 376–378 (2008).
 14. Okada, H. *et al.* Superconductivity under high pressure in LaFeAsO . *J. Phys. Soc. Jpn.* **77**, 113712 (2008).
 15. Igawa, K. *et al.* Pressure-Induced Superconductivity in Iron Pnictide Compound SrFe_2As_2 . *J. Phys. Soc. Jpn.* **78**, 025001 (2009).
 16. Okabe, H. *et al.* Pressure-induced high- T_c superconducting phase in FeSe : Correlation between anion height and T_c . *Phys. Rev.* **B 81**, (2010) 205119.
 17. Aichhorn, M. *et al.* Importance of electronic correlations for structural and magnetic properties of the iron pnictide superconductor LaFeAsO . *Phys. Rev.* **B 84**, (2011) 054529.
 18. Lee, C. H. *et al.* Relationship between crystal structure and superconductivity in iron-based superconductors. *Solid State Commun.* **152**, 644–648 (2012).
 19. Takahashi, H. *et al.* Pressure studies of $(\text{La}, \text{Sm})\text{FeAsO}_{1-x}\text{F}_x$ and LaFePO . *Physica C* **469**, 413 (2009).
 20. Drotzinger, S. *et al.* Pressure versus concentration tuning of the superconductivity in $\text{Ba}(\text{Fe}_{1-x}\text{Co}_x)_2\text{As}_2$. *J. Phys. Soc. Jpn.* **79**, 114705 (2010).
 21. Onari, S. *et al.* High- T_c superconductivity near the anion height instability in Fe-based superconductors: Analysis of $\text{LaFeAsO}_{1-x}\text{H}_x$. *Phys. Rev. Lett.* **112**, 187001 (2014).
 22. Suzuki, K. *et al.* Model of the electronic structure of electron-doped iron-based superconductors: evidence for Enhanced Spin Fluctuations by Diagonal Electron Hopping. *Phys. Rev. Lett.* **113**, 027002 (2014).
 23. Blöchl, P. E. Projector augmented-wave method. *Phys. Rev. B* **50**, 17953–17979 (1994).
 24. Kresse, G. & Furthmüller, J. Efficient iterative schemes for ab initio total-energy calculations using a plane-wave basis set. *Phys. Rev. B* **54**, 11169–11186 (1996). (1996).
 25. Perdew, J. P. *et al.* Restoring the Density-Gradient Expansion for Exchange in Solids and Surfaces. *Phys. Rev. Lett.* **100**, 136406 (2008).
 26. Matsuishi, S. *et al.* Controlling factors of T_c dome structure in 1111-type iron arsenide superconductors. *Phys. Rev.* **B89**, 094510-1 - 5 (2014).

Acknowledgements

This work was partly supported by JSPS Grants-in-Aid for Scientific Research (B) (24340088) and the Strategic Research Base Development Program for Private Universities (2009, S0901022) of MEXT. The research at Tokyo Tech was supported by the MEXT Element Strategy Initiative to form a Core Centre and JSPS FIRST Project.

Author information

Reprints and permissions information are available at www.nature.com/reprints.

Correspondence and requests for materials should be addressed to

H.T. (hiroki@chs.nihon-u.ac.jp).

Author contributions

H.T. and H.H. planned the research. S.I., Y.M. and S.M. performed the high pressure synthesis. H.S., N.N., C.K. and T.N. carried out high-pressure measurement. S.I. and S.M. performed DFT calculations. H.T., H.H., S.I. and H.S. discussed the results and wrote the manuscript.

Competing financial interests

The authors declare no competing financial interests.

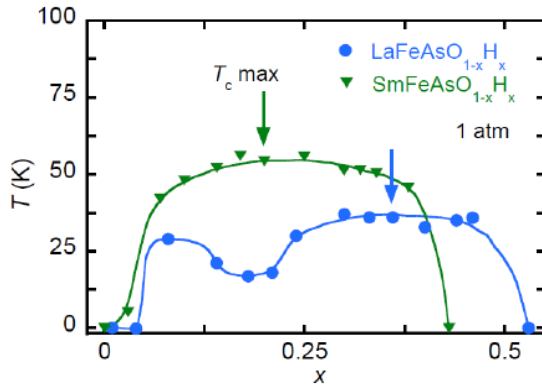


Figure 1. Phase diagram in hydrogen-doped 1111 materials

Superconductive phase diagrams for $LnFeAsO_{1-x}H_x$ ($Ln = La$ and Sm). A double-dome $T_c(x)$ is observed in $LaFeAsO_{1-x}H_x$ ⁷. The two kinds of superconducting phases, SC1 and SC2, are thought to have different origins. The arrows show the maximum T_c , which shifts to the lightly-doped side in the order La to Sm. This shift in T_c -dome is observed for $LnFeAsO_{1-x}H_x$ ($Ln = La, Ce, Sm, \text{ and } Gd$) in the order La to Gd, i.e., in order of decreasing ionic radius.

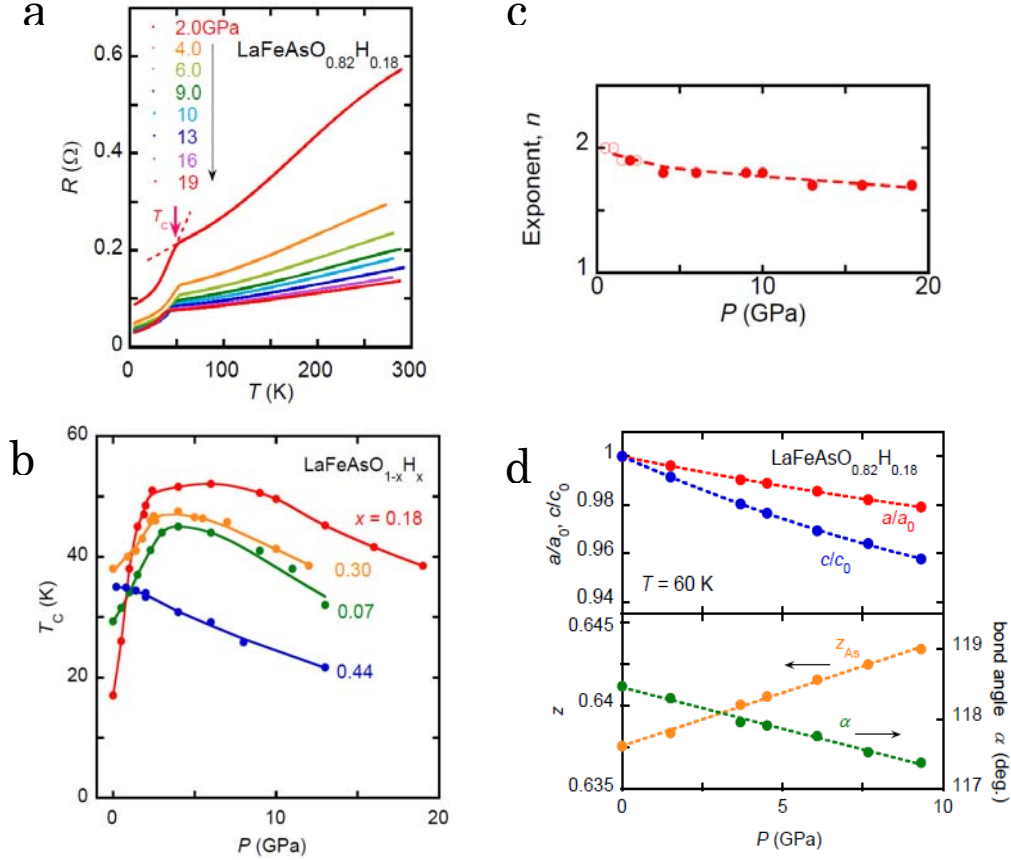


Figure 2. **Superconducting and structural properties in $\text{LaFeAsO}_{1-x}\text{H}_x$ under high pressure**

- a)** Temperature dependence of the electrical resistance for $x = 0.18$ using DAC. The onset T_c is determined to be the intersection of two extrapolated lines, one drawn just above T_c on the resistance curve in the normal state and the other drawn through the steepest part of the resistance curve in the superconducting state. These extrapolated lines are shown on the data for 2 GPa. The superconducting transition is clearly observed for each measurement, although the zero resistance is not observed down to 4 K. **b)** Pressure dependence of T_c for $x = 0.07, 0.18, 0.30, \text{ and } 0.44$. The T_c is defined as the onset temperature of the transition. Solid curves are a guide for the eye. **c)** Pressure dependence of n for $x = 0.18$. The n value decreases slightly under high pressure. **d)** Pressure dependence of lattice constants normalized to the ambient pressure values, z_{As} and As-Fe-As angle α . The lattice constants are obtained by high-pressure X-ray diffraction, and the atomic positions are estimated by DFT calculations using the experimental lattice constants.

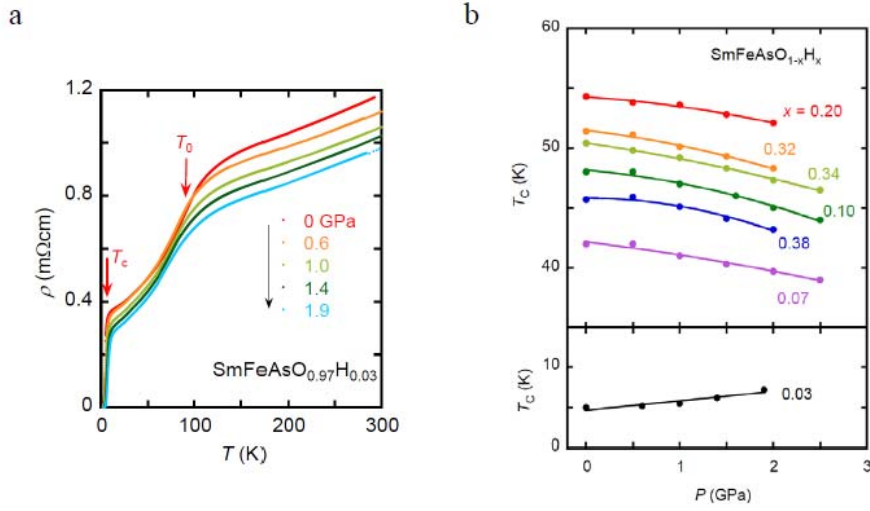


Figure 3. **Superconducting properties in $\text{SmFeAsO}_{1-x}\text{H}_x$ under high pressure**

a) Temperature dependence of electrical resistivity for $x = 0.03$, obtained using the piston-cylinder device. The anomalous decrease in resistivity observed around 100 K corresponds to structural and magnetic transitions. The transition temperature T_0 is determined as the temperature that shows the peak $d\rho/dT$ value and decreases with increasing pressure with an initial slope of -10.0 K/GPa. It is indicated by arrows on the data for 0 GPa. The superconducting transition temperature is also observed at around 5 K and increases with pressure. **b)** Pressure dependence of T_c for $x = 0.03, 0.07, 0.10, 0.20, 0.32, 0.34$, and 0.38 . The T_c is defined as the onset temperature of the transition. Solid curves are a guide for the eye.

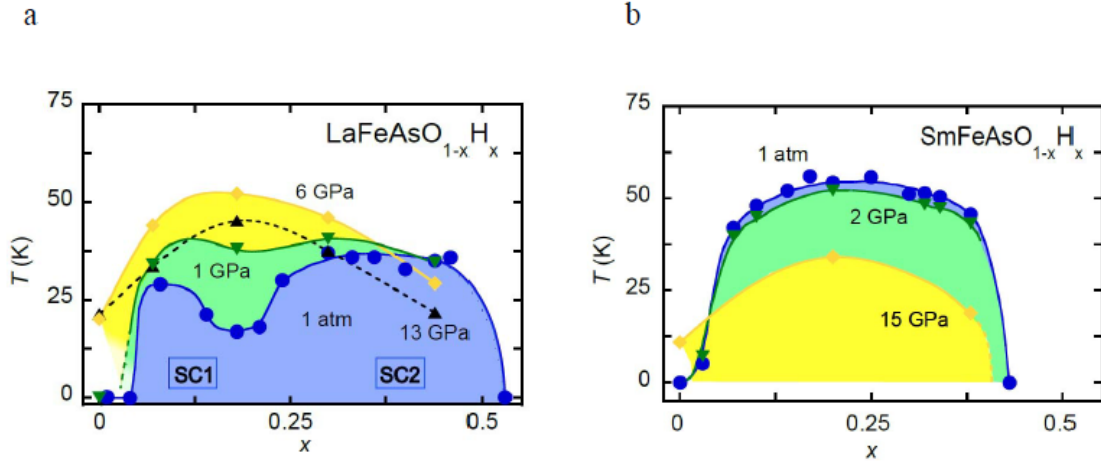


Figure 4. **Phase diagram in $\text{LaFeAsO}_{1-x}\text{H}_x$ and $\text{SmFeAsO}_{1-x}\text{H}_x$ under high pressure**

a) The phase diagrams of $\text{LaFeAsO}_{1-x}\text{H}_x$ under the pressures 1 atm and 1, 6, and 13 GPa. As the pressure is increased to 6 GPa, the T_c -valley is greatly raised and the T_c dome SC2 shifts to the lightly-doped side. A large enhancement in T_c to 52 K is observed at the T_c -valley. The T_c dome is suppressed above 6 GPa. **b)** The phase diagrams of $\text{SmFeAsO}_{1-x}\text{H}_x$ for the pressure of 1 atm and 2 and 15 GPa. T_c is suppressed upon the application of pressure, except in the case of the undoped material. Pressure-induced

superconductivity has previously been identified in undoped SmFeAsO by our group¹⁹. The single T_c dome seems to shift to the lightly-doped side under high pressure. The same trend is seen in the case of LaFeAsO_{1-x}H_x.